Effect of Variation in Equilibrium Shape on ELMing H–Mode Performance in DIII–D Diverted Plasmas

M.E. Fenstermacher,[1] T.H. Osborne,[2] T.W. Petrie,[2] C.J. Lasnier,[1] A.W. Leonard,[2] J.G. Watkins,[3] T.N. Carlstrom,[2] R.J. Groebner,[2] A.W. Hyatt,[2] R.J. La Haye,[2] M.A. Mahdavi,[2] G.D. Porter,[1] S.L. Allen,[1] J.A. Boedo,[4] N.H. Brooks,[2] R.J. Colchin,[5] R. Maingi,[5] M.E. Rensink,[1] T.L. Rhodes,[6] D.M. Thomas,[2] M.R. Wade,[5] W.P. West,[2] D.G. Whyte,[4] N.S. Wolf,[1] and the DIII–D Team

[1]Lawrence Livermore National Laboratory, Livermore, California 94550, USA
[2]General Atomics, P.O. Box 85608, San Diego, California 92186-5608, USA
[3]Sandia National Laboratories, Albuquerque, New Mexico 87185-5800, USA
[4]University of California, San Diego, La Jolla, California 92093-0319, USA
[5]Oak Ridge National Laboratory, Oak Ridge, Tennessee 37831, USA
[6]University of California, Los Angeles, California 90024-1597, USA

E-mail contact of main author: max.fenstermacher@gat.com

Abstract. The changes in the performance of the core, pedestal, scrape-off-layer (SOL), and divertor plasmas as a result of changes in triangularity, δ, up/down magnetic balance, and secondary divertor volume were examined in shape variation experiments using ELMing H–mode plasmas on DIII–D. In moderate density, unpumped plasmas, high $\delta \sim 0.7$ increased the energy in the H–mode pedestal and the global energy confinement of the core, primarily due to an increase in the margin by which the edge pressure gradient exceeded the value which would have been expected had it been limited by infinite-n ideal ballooning modes. In addition, a nearly balanced double-null (DN) shape was effective for sharing the peak heat flux in the divertor in these attached plasmas. For detached plasmas good heat flux sharing was obtained for a substantial range of unbalanced DN shapes. Finally, the presence of a second X–point in unbalanced DN shapes did not degrade the plasma performance if it was sufficiently far inside the vacuum vessel. These results indicate that a high δ unbalanced DN shape has some advantages over a single null shape for future high power tokamak operation.

1. Introduction

This paper describes experiments that have increased our understanding of the complex coupling of core plasma performance to plasma cross section and divertor plasma shape. The choice of the plasma shape is made very early in the design of any future tokamak [1] and it can have significant implications for plasma performance. To obtain more complete understanding of these effects, systematic shape variation experiments were done using ELMing H–mode plasmas in DIII–D. The response of core, pedestal, scrape-off-layer (SOL), and divertor plasma performance was examined versus triangularity, δ, up/down magnetic balance, dR_{sep}, and secondary divertor volume, Z_x^s. Here dR_{sep} is the midplane radial distance between the upper and lower divertor separatrices. The primary divertor separatrix is the boundary of the closed flux surfaces of the core; the secondary divertor separatrix maps to a flux surface that is radially outboard of the primary at the midplane. Z_x^s is the height of the secondary divertor X-point and is a measure of the volume occupied by the secondary divertor. The focus of the experiments was to determine if: (1) increased triangularity improved performance, (2) nearly balanced double-null (DN) shapes had advantages over single-null (SN) shapes and (3) the minimum volume required for the secondary divertor (that will likely appear inside the vacuum vessel for future high triangularity designs), could be predicted.

The paper is organized as follows. Section 2 describes the setup of the experiments including examples of typical time histories of the discharges and definitions of the parameters that were varied in the shape studies. Results are given in Section 3 with separate subsections for the variations in δ, dR_{sep}, and Z_x^s. In each case the behavior at typical H–mode density is contrasted with the behavior at high density using gas injection. Conclusions are given in Section 4.

2. Description of Experiments

Systematic studies of the effect of shape variation in both moderate and high density regimes were done by varying the shape from one discharge to the next and varying the density within the discharge using gas injection. In addition, a small number of the discharges had constant injected power and gas puff with a variation in plasma shape to examine the effect of shape variation without shot-to-shot variability. Examples of the evolution of both types of discharges are shown in Fig. 1. Type I ELMing H–mode plasmas [2] were studied; this complements previous shape studies [3] in VH–mode plasmas [4]. Typical plasma parameters (and the ranges used in some of the studies) were: plasma current, I_p = 1.4 (0.8–2.0) MA, toroidal field, B_T = 2.0 (1.4–2.1) T, major radius, R_0 = 1.68 m, minor radius, a = 0.6 m, elongation, κ = 2.0 (1.7–2.2), injected neutral beam power, P_{inj} = 5 (2–7) MW, and safety factor at 95% flux, q_{95} = 4.5 (2.25–10). For most of the studies the shape, current flattop, injected power, and H–mode density levels were established within the first 2 s of the discharge. Gas was then injected within the remaining 3.5 s to produce a density ramp from typical H–mode density $n_e/n_G \sim 0.5$, where n_G is the Greenwald density [5], to the H–L back transition density limit [Fig. 1(a)]. Well diagnosed discharges with constant input conditions and variation of the shape within the discharge [Fig. 1(b)] were obtained only in the dR_{sep} variation studies.

Shape variation studies were performed by systematically varying one of the three shape parameters, δ, dR_{sep}, or Z_x^s, while holding the other two as constant as possible. Descriptions of these parameters are illustrated in Fig. 2. The nominal values were δ = 0.7, dR_{sep} = 0, and Z_x^s = 16 cm. The triangularity variations [Fig. 2a(i,ii)] were performed by varying the upper triangularity from δ = 0 to 0.7 in a plasma magnetically unbalanced toward a lower single-null (LSN), dR_{sep} = –4 cm, with Z_x^s = 11 cm. The magnetic balance variations [Fig. 2(b)] used dR_{sep} = –4.5 to +4.5 cm with δ and Z_x^s at the nominal values and the secondary divertor volume studies [Fig. 2(c)] varied Z_x^s from 1.0 to 17.5 cm with dR_{sep} = 0.5 cm and δ at the nominal value.

3. Results

A. Triangularity variation

Increasing the triangularity of the plasma cross section improves the performance of the core plasma both in terms of energy confinement and beta limit. To quantify the effect of δ, SN

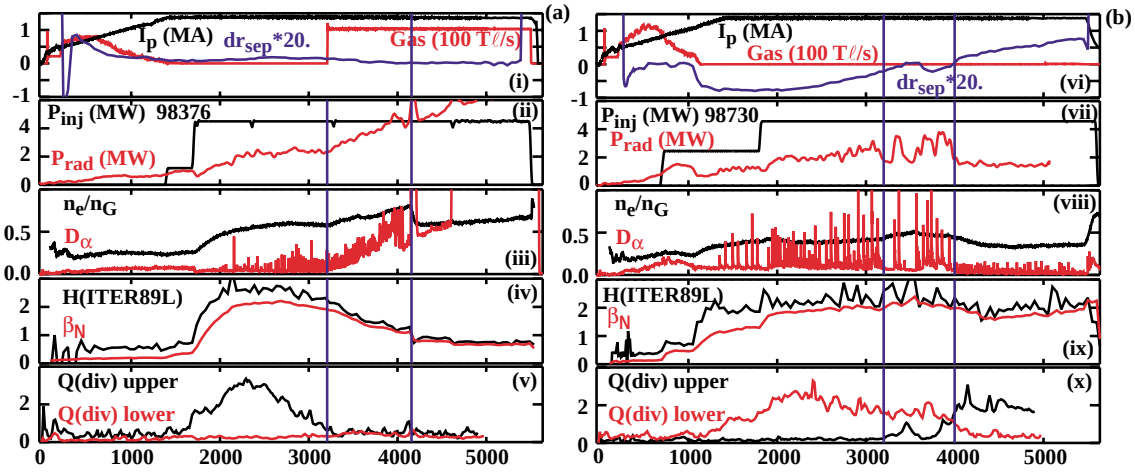

FIG. 1. Evolution of discharge parameters for two types of discharges used in these experiments: (a) constant plasma shape with gas injection and density ramp, (b) constant injected power and gas with up/down magnetic balance variation (dR_{sep}). Parameters are: (i), (vi) plasma current, I_p (MA), gas injection (100 Tl/s), dR_{sep} (20 cm), (ii), (vii)) injected neutral beam power, P_{inj} and radiated power, P_{rad} (MW), (iii), (viii) line-averaged density normalized to Greenwald density and D_a emission (iv), (ix) energy confinement normalized to ITER89 L-scaling, H(ITER89L) and normalized beta, $\beta_N = \beta/(I_p/aB_T)$, and (v), (x) upper and lower peak heat flux Q(div) (MW/m^2)

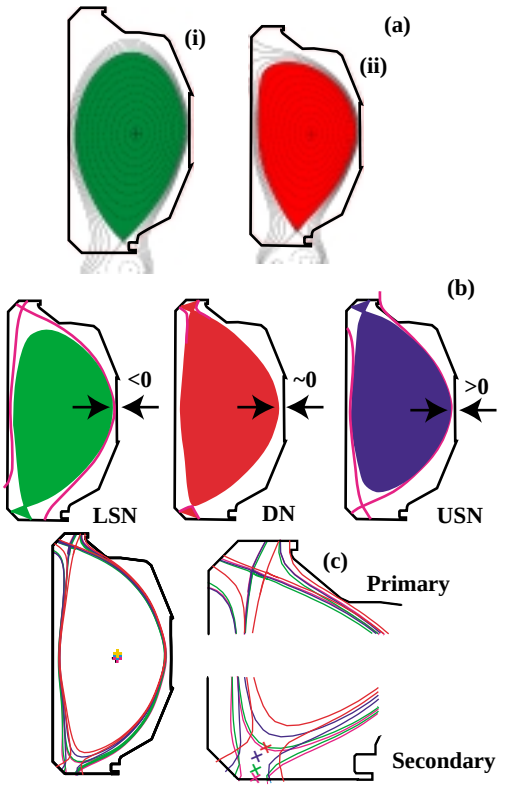

FIG. 2. Plasma shapes used in these experiments. (a) Shapes from triangularity variations: (ai) low triangularity and (aii) high triangularity, (b) from up/down magnetic balance studies and (c) from secondary X-point height variations (expanded divertor views shown).

discharges were used with fixed lower X–point position and upper triangularity varied from 0.0 to 0.7 [Fig. 2a(i,ii)]. The performance improvement varied with the density regime of operation as described below.

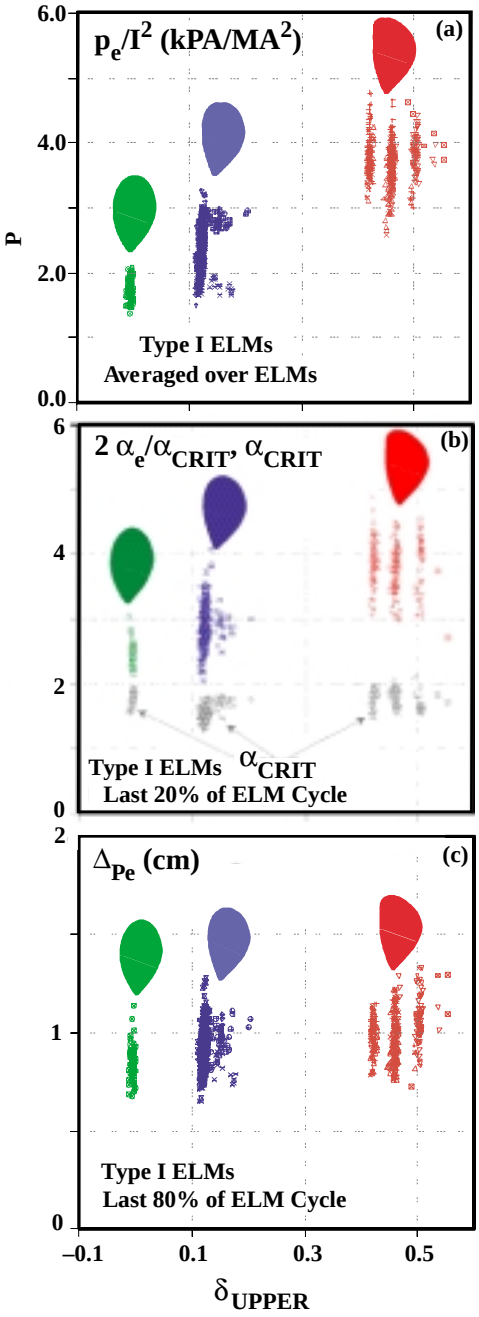

FIG. 3. Effect of upper triangularity δ on the H–mode pedestal at moderate density. (a) Electron pressure at the top of the H–mode transport barrier showing a strong increase with δ, (b) edge pressure gradient normalized to ballooning mode limit and value of α_{crit}, (c) width of the steep edge electron pressure gradient region, Δ_{pe},.

Results at Typical H–Mode Density. The δ variations in unpumped plasmas at low to moderate density, ($n_e/n_G \leq 0.7$) showed that the core and pedestal performance improve with δ (Fig. 3) [6]. The pressure at the top of the H–mode pedestal, p^{ped}, increased strongly with δ [Fig. 3(a)]. This pressure increase was due primarily to an increase in the edge pressure gradient α_e[Fig. 3(b)]. The width of the edge pressure pedestal Δ_{pe} [Fig. 3(c)] and the ideal ballooning mode stability limit, α_{crit} [Fig. 3(b)] remained nearly constant. In each case the edge pressure gradient exceeded α_{crit} by a large margin [6]. Access to the second stability regime for ideal ballooning modes may explain the observation of pressure gradients in excess of the ballooning mode limit [6,7]. The normalized energy confinement, $H = \tau_E/\tau_E^{ITER89P}$, increased with δ as a result of the increase in the pedestal energy.

The width of the H-mode transport barrier, Δ, normalized to a fixed shape scaling showed a weak δ dependence [6]. Previous experiments at fixed plasma shape [8] tested the measured edge pedestal width against theoretical models by varying the edge pedestal temperature using gas puffing and divertor pumping. No explicit dependence on T_e^{ped} was found. Instead the width scaled as $\Delta \propto \left(\beta_p^{ped}\right)^{1/2}$. The width of the pressure pedestal at low δ in Fig. 3(c) is above this scaling prediction and at high δ the width is below this scaling. This suggests an inverse dependence on δ.

Triangularity Dependence at High Density. At high density, ($n_e/n_G \sim 1$), the performance variation with δ at fixed profiles was weak [9]. Figure 4 shows that over a wide range of densities ($n_e/n_G < 0.7$) the pedestal pressure prior to an ELM was very nearly constant but depended on plasma shape consistent with Fig. 3(a). As density was increased, p^{ped} began to decrease in the range $0.6 < n_e^{ped}/n_G < 0.8$ in both low and high δ discharges. Once the reduction in p^{ped} began it was observed to decay at a rate described by $\partial p^{ped}/\partial n \propto \eta^{-0.5}$, where η is the pedestal resistivity. This scaling was independent of δ. Therefore, since p^{ped} and T^{ped} are higher in the higher δ shape for the density at which p^{ped} begins to decrease [Fig. 4(b)], the decay of p^{ped} with increasing density was more rapid [Fig. 4(b)] than in the lower δ case [Fig. 4(a)]. This leads to the weak dependence of pedestal pressure on δ at high $n_e/n_G \sim 1$. However, both the change in pedestal pressure and the response of the density profile play a role in setting the energy confinement. The low δ discharges at high density with divertor pumping showed central density peaking leading to recovery of good confinement [9].

ELM Behavior Versus Triangularity. For low to moderate density discharges the energy loss for Type I ELMs was a fixed fraction of the pedestal energy [10] independent of triangularity; the fraction was lower at high density. As the pedestal energy increased with δ for $n_e/n_G \leq 0.7$ in the shaping experiments [Fig. 3(a)], so did the energy lost with each ELM. In high density $n_e/n_G > 0.7$ LSN discharges with active pumping of the private flux region, high frequency, low energy Type I ELMs were produced [11]. The ELM energy, calculated from fast magnetics measurements, was a substantially lower fraction of the pedestal energy than the previous scaling [10] derived from lower density discharges (Fig. 5). At sufficiently high density, similar low energy ELMs were produced in discharges with either low or high upper triangularity. The minimum pedestal density to achieve ELMs with energy below the previous scaling seemed to be higher for the high upper triangularity case [Fig. 5(a)]. The normalized ELM energy decreased for both the low and high triangularity cases at a similar pedestal temperature [Fig. 5(b)]. The low energy ELM perturbed only the pedestal density (not the pedestal temperature) in the high density cases; for low density the ELMs perturb both the pedestal density and temperature. This produces a much lower edge pedestal pressure drop during the ELMs at high density.

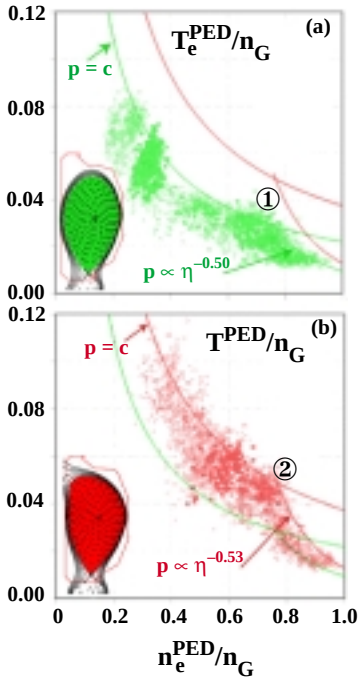

FIG. 4. Effect of triangularity δ on H–mode pedestal density and temperature. At low δ (a) the edge ballooning limit (green curve) is lower then at high δ (b) (red curve). As the pedestal density is increased by gas puffing the pedestal pressure decreases as the square root of resistivity η starting at the same density (a-1, b-2).

B. Up/down magnetic balance

In principle, balanced double-null operation could improve the performance of the divertor by reducing the peak heat load to the targets by a factor of two. The disadvantage of DN shapes is that present design concepts use more of the volume inside the toroidal field coils for divertor plasma and less for the burning core plasma that SN shapes.

Heat and Particle Flux Sharing at Typical H–Mode Density. The up/down magnetic balance studies at low to moderate density showed that the distribution of the heat flux to attached divertors can be predicted from knowledge of the flux surface geometry and midplane SOL power scale widths [12,13]. For attached plasmas, the variation in heat flux sharing between divertors is large for small changes in dR_{SEP} near 0, i.e., near DN (Fig. 6). This sharp dependence however may actually be useful in feedback schemes to control DN shapes. This sensitivity is consistent with the measured midplane scrape-off width of the parallel divertor heat flux, λ_q. Furthermore, λ_q can be approximated to within a factor of two with a simple model using only the midplane scrape-off lengths of n_e and T_e. This suggests that divertor processes (e.g., recycling) are not dominating the physics.

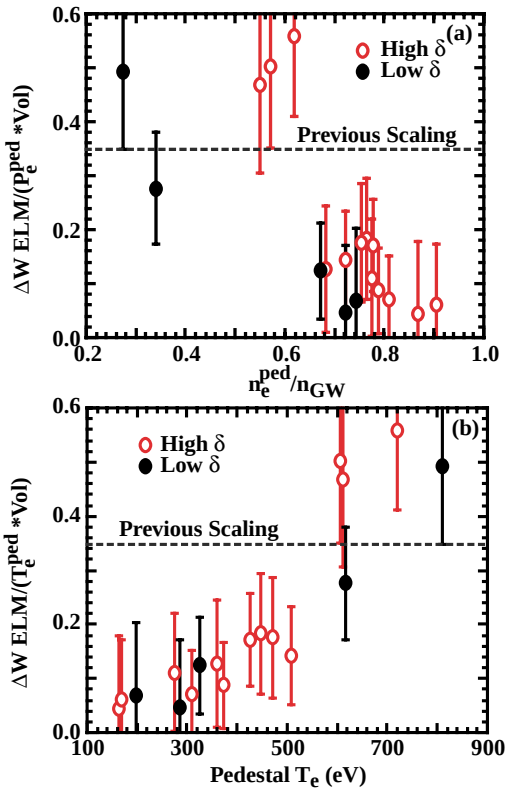

FIG. 5. Fraction of the pedestal electron energy lost at each ELM as a function of (a) pedestal density and (b) pedestal temperature.

Other effects of changes in magnetic balance can not be predicted from flux surface geometry alone. The variation of the peak particle flux between attached divertors is less sensitive to changes in dR_{SEP} than in the heat flux case (Fig. 6). This suggests that divertor processes are much more important in this case. Neutral recycling from the target plates tends to broaden the resulting particle flux profile on the plates when the neutral mean free path is comparable to the width of the incoming ion flux profile. This divertor effect decouples somewhat the peak particle flux at the target from the incoming ion flux profile thereby reducing the sensitivity of peak target particle flux to dR_{SEP} variation.

Magnetic Balance Dependence at High Density. As the plasma density is increased to near the H–L back transition density, the sensitivity of the peak heat flux balance to dR_{SEP} variation is reduced and a dependence of the back transition density on dR_{SEP} is observed (Fig. 7). At high density the divertor plasma is detached from the target surfaces and the heat flux profile is dominated by local effects in the divertor (radiation, recombination, convection etc.) rather than by conduction along field lines as in the attached case. The target peak heat flux is not strongly coupled to the SOL heat flux profile under detachment conditions and the sensitivity to changes in dR_{SEP} is reduced. When the density is pushed to the H–L back transition limit, variation of dR_{SEP} shows a significantly lower transition density for magnetic balance away from the ion ∇B drift direction (Fig. 7).

ELM Heat Flux Sharing. Variations in up/down magnetic balance of attached plasmas show that the shift of the ELM energy flux from one divertor to the other is much more gradual with shape change [14] than the shift of the time averaged heat flux (Fig. 8). The shift width of the ELM peak energy density is 1.9 cm in dR_{SEP} compared with a shift width of 0.4 cm for the peak time averaged heat flux in attached plasmas. Energy density profiles on the targets during ELMs confirm that the profiles are up to five times broader than the profile of the time averaged heat flux. The ELM shift width is comparable to the shift width or the peak time averaged heat flux in detached plasmas and the shift width of the particle flux. In contrast to the reasons for the broad shift width of the particle flux and time-averaged heat flux in high density plasmas, the broad shift width of the ELM energy density is likely due to broad deposition of the ELM energy in the SOL at the midplane which then propagates along field lines to the divertor.

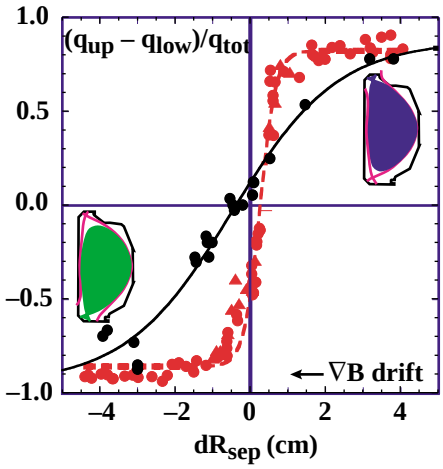

FIG. 6. Peak heat flux sharing (red) and peak particle flux sharing (black) as functions of up/down magnetic balance for moderate density plasmas. The vertical axis is value in the upper divertor minus the lower divertor normalized to the total.

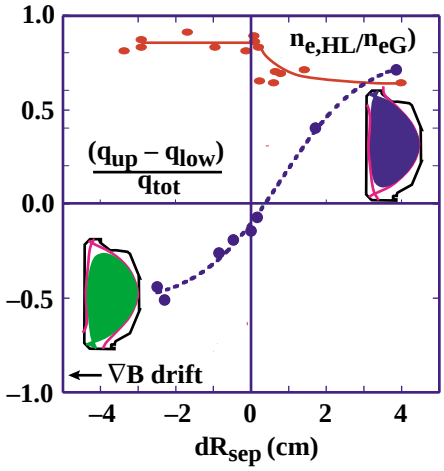

FIG. 7. Peak heat flux sharing (blue) and line averaged density normalized to the Greenwald density at the H–L back transition (red) as functions of up/down magnetic balance for high density plasmas.

C. Minimization of secondary divertor volume

Systematic reductions of the volume of the secondary divertor were done to determine the minimum volume consistent with good core and divertor performance. The performance sensitivity (Fig. 9) was examined by varying the secondary X–point height from the target plate while holding the primary X–point height fixed [Fig. 2(c)]. The ion ∇B drift was in the direction of the primary divertor.

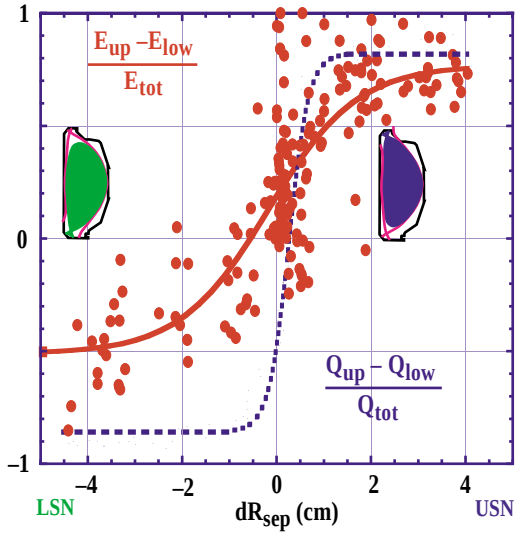

FIG. 8. ELM energy sharing (red) as a function of up/down magnetic balance shifts more gradually with dR_{sep} variation than time-averaged peak heat flux (blue).

Peak Divertor Heat Flux and Core Fueling. For an unbalanced DN plasma, the divertor heat flux did not increase as the secondary divertor volume was reduced provided the secondary X–point was well inside the vessel [15]. This indicates that the distribution of power in the SOL is unaffected by X–point height variation until the high cycling character of one of the divertors is lost at small X–point height. The re-normalized peak heat flux in the secondary divertor as a function of Z_x^s is shown in Fig. 9(a) for the pre-gas ELMingH–mode phase of unpumped plasmas. Details of the re-normalization procedure that removes the effects of dR_{SEP} variation in this dataset are given in Ref. [15]. A value of 1.0 in Fig. 9(a) indicates the peak heat flux in the secondary divertor is the expected value for Z_x^s = 16 cm consistent with Fig. 6, a value less than (greater than) 1.0 means the secondary divertor is getting less than (greater than) the expected heat flux. Figure 9(a) shows that for high Z_x^s ~8-16 cm the heat flux was the expected value. As Z_x^s was reduced, the normalized peak heat flux in the secondary divertor decreased due to flux expansion. However, for low Z_x^s ~ 1-2 cm the peak heat flux was significantly larger than the expected value because the high recycling character of the secondary divertor was lost at low Z_x^s.

Core performance was also affected [15] as secondary divertor volume was reduced [Fig. 9(b)]. The effective rate of rise of the core density at the L–H transition increased as

Z_x^s was reduced. This core fueling rate increase was about a factor of two as Z_x^s was reduced from 17 to 1 cm taking the dataset as a whole. The large scatter in the data is due in part to changing wall conditions in these discharges. The trend however is consistent with the higher core penetration probability of neutrals born in the secondary divertor as the distance from the target surface to the last closed flux surface decreased.

Density Limits. The maximum line averaged H–mode density, before the H–L back transition, decreased as secondary X–point height decreased [Fig. 9(c)]. The absolute density in the unpumped discharges was lower than with pumping at high Z_x^s. However, the density limit dropped more rapidly with Z_x^s reduction in the pumped cases yielding similar results at low Z_x^s. The width of the edge density pedestal was larger in the unpumped plasmas indicating a greater penetration of neutrals without pumping. The dominant physics that explains this trend is again the increase in neutral escape probability from the secondary divertor as Z_x^s was reduced. In this case the effect of increased neutral ionization in the edge of the core is to lower the pedestal temperature for fixed core density as Z_x^s was reduced thereby inducing the H-L back transition at lower core density. This process also explains the higher density limit with pumping at moderate to high Z_x^s.

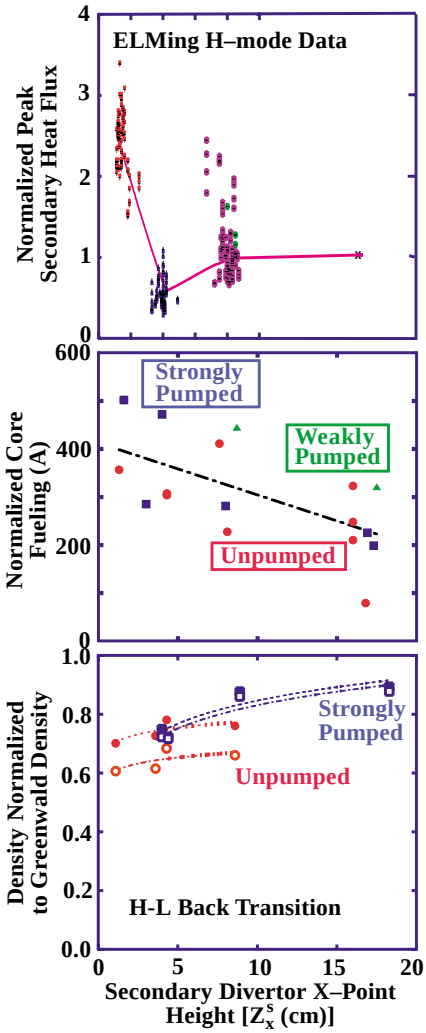

FIG. 9. Effects of variation in volume of the secondary divertor for unbalanced DN shapes. (a) Ratio of the peak heat flux measured in the secondary divertor to that expected from the high X–point shapes used in Fig. 6 as a function of secondary X–point height. Data is from the ELMing H–mode phase of three different discharges. (b) Effective fueling rate of the core plasma at the L–H transition for unpumped (red circles), weakly pumped (green triangles) and strongly pumped (blue squares) discharges. (c) Line-averaged density (closed symbols) and pedestal density (open symbols) at the H–L back transition normalized to Greenwald density for unpumped (red circles) and strongly pumped (blue squares) discharges.

4. Discussion and Conclusions

Optimization of the plasma shape in designs of future high power tokamaks involves a combination of many performance trade-offs. The data obtained in these experiments examined the sensitivity of core and divertor performance to δ, dR_{sep}, and Z_x^s and density regime. At moderate density in unpumped plasmas increasing δ increased the core energy confinement by increasing the energy in the edge pedestal. The trade-off was that the ELM energy also increased proportionately with the pedestal energy; this could make divertor design more difficult. At high density the ELM energy was reduced (frequency increased) but at the expense of confinement. With divertor pumping good energy confinement was restored at high density with peaking of the core density profile [9]. However the pumped data did not give a clear indication that high triangularity was an advantage.

At moderate density in unpumped plasmas, the magnetic balance required for balancing the peak heat flux between the two divertors of a DN shape was slightly shifted toward the divertor with the ion ∇B drift out of the divertor. This asymmetry is consistent with ∇B and ExB drift effects [13]. However, at high density this configuration produced a lower density limit at the H-L back transition than for magnetic balance shifted toward the divertor in the ion ∇B drift direction. At moderate density, the shift of the heat flux from one divertor to the other was

very sensitive to the magnetic balance indicating that a strict control requirement would be necessary to share the heat flux between divertors. However, this strong sensitivity might also be an advantage in coil feedback schemes for controlling the magnetic balance by monitoring the divertor heat flux balance. The heat flux sharing at high density, the particle flux sharing, and the ELM energy sharing were all much less sensitive to magnetic balance so they would not be the dominant factors in the dR_{sep} control requirements for future devices. The data also indicated that the ELM energy deposition profile in the divertor was broader that the profile of the time averaged heat flux so the ELMs would be the factor that determines how close divertor baffles can be to the SOL and divertor plasma fan.

Reduction of the secondary divertor volume to allow more volume for the burning core plasma produces both advantages and disadvantages to performance. At moderate density in unpumped plasmas the peak heat flux in the secondary divertor can be reduced but the fueling rate of the core plasma increases and the high density limit at the H–L back transition is lowered. This may produce a reduction in the density operating window for unpumped plasmas that may be ameliorated somewhat by pumping.

In conclusion the quantitative understanding gained here provides valuable guidance as to the effect of shape variations on projected H–mode performance in future tokamaks. High core performance at moderate density can be obtained with high δ core plasma. Favorable divertor performance can also be obtained at high δ in unbalanced DN divertors at moderate density and the minimum divertor volume and magnetic balance requirements are predictable. These results indicate that for high δ H-mode operation an unbalanced DN shape has some advantages over a single null shape for future high power tokamak operation.

Acknowledgments

This work was supported by the U.S. Department of Energy under Contract Nos. DE-AC03-99ER54463, W-7405-ENG-48, DE-AC04-94AL85000, DE-AC05-96OR22465, and Grant Nos. DE-FG03-86ER53225 and DE-FG03-95ER54294.

References

[1] ITER Physics Basis Editors, et al., Nucl. Fusion **39**, (1999) 2137.
[2] ZOHM, H., et al., Plasma Phys. and Control. Fusion **38**, (1996) 1497.
[3] LAZARUS, E.A., et al., Proc. 15th Int. Conf. on Plasma Physics and Controlled Nuclear Fusion Research, Seville, Spain, 1994, IAEA-CN-60/A5-1, IAEA, Vienna, Vol. 1, (1995) 609
[4] JACKSON, G.L., et al., Phys. Rev. Lett. **67** (1991) 3098.
[5] GREENWALD, M., et al., Nucl. Fusion **28** (1988) 2199.
[6] OSBORNE, T.H., et al., Plasma Phys. and Control. Fusion **42**, 1, (2000).
[7] MILLER, R.L., et al., Plasma Phys. and Control. Fusion **40**, 753 (1998).
[8] OSBORNE, T.H., et al., J. Nucl. Mater. **266-269**, 131 (1999).
[9] OSBORNE, T.H., et al., "Gas Puff Fueled H–Mode Discharges with Good Energy Confinement Above the Greenwald Density Limit in DIII–D," Proc. 14th Int. Conf. on Plasma Surface Interactions, Rosenheim (to be published in J. Nucl. Mater.).
[10] LEONARD, A.W., HERRMANN, A., ITAMI, K., et al., J. Nucl. Mater. **266-269**, 109 1999.
[11] LEONARD, A.W., et al., "Tolerable ELMs at High Density in DIII-D," Proc. 14th Int. Conf. on Plasma Surface Interactions, Rosenheim (to be published in J. Nucl. Mater.).
[12] PETRIE, T.W., et al., Contr. Fusion and Plasma Phys. **23J**, 1237 (1999).
[13] PETRIE, T.W., et al., "The Effect of Divertor Magnetic Balance on H–Mode Performance in DIII–D," Proc. 14th Int. Conf. on Plasma Surface Interactions, Rosenheim (to be published in J. Nucl. Mater.).
[14] LASNIER, C.J., et al., "Effect of Magnetic Geometry on ELM Heat Flux Profiles," Proc. 14th Int. Conf. on Plasma Surface Interactions, Rosenheim (to be published in J. Nucl. Mater.).
[15] FENSTERMACHER, M.E., et al., "Performance of High Triangularity Plasmas as the Volume of the Secondary Divertor is Varied in DIII-D," Proc. 14th Int. Conf. on Plasma Surface Interactions, Rosenheim (to be published in J. Nucl. Mater.).